Chiral Surfactants for Dispersing Carbon Nanotubes

Journal:	*Polymer Chemistry*
Manuscript ID:	PY-ART-01-2015-000040.R1
Article Type:	Paper
Date Submitted by the Author:	22-Feb-2015
Complete List of Authors:	Lin, Pengcheng; Northeastern University, Cong, Yuehua; Northeastern University, Zhang, Baoyan; Northeastern University,

Polymer Chemistry

RSCPublishing

PAPER

Chiral Surfactants for Dispersing Carbon Nanotubes

Pengcheng Lin, Yuehua Cong and Baoyan Zhang*

A novel and effective way to disperse carbon nanotubes (CNTs) by using amphiphilic chiral side-chain liquid crystalline oligomers (ACSLCOs) as chiral surfactants, which possess dual affinity with both CNTs and chiral liquid crystals (CLCs) is reported here for the first time. As for the binary system consisting of CNTs and ACSLCOs, the concentration of CNTs dispersed by ACSLCOs is determined by fourier transform infrared (FTIR) spectrum combined with ultraviolet-visible-near infrared spectrum, the ability to disperse CNTs increases with the increase of mole fraction of polycyclic conjugated structure on chiral surfactants and the concentration reaches 0.85 mg mL^{-1}. The dispersion state of CNTs in the composites is characterized by FTIR imaging system with CNT-O7 composite demonstrating the best dispersion of CNTs. The evenly dispersed CNTs reduce the glass transition temperature and improve the thermal stability of ACSLCOs. As for the ternary system consisting of CNT, O7 and low molecular weight CLC, the dispersion state of CNTs is characterized by polarized optical microscope. Result shows CNTs possess excellent compatibility with low molecular weight CLCs with the assist of O7. The dispersed CNTs are proved to have increased the chiral stability of chiral host by the measurement of bragg selective reflection.

Introduction

Carbon nanotubes (CNTs) have drawn extensive attention since Iijima reported in 1991.[1] They have presented great potential in applications, such as energy storage,[2,3] displays,[4] high-performance electronics,[5-7] biological sensing[8,9] and asymmetric chemical synthesis.[10] However, CNTs bundle and cluster together in disordered agglomerates due to the integral interaction energy and van der Waals force between neighboring CNTs.[11-14] In order to take full advantage of their highly anisotropic thermal, electrical, and optical characteristics, the nanotubes are required to be dispersed. Various effective methods have been established to achieve homogeneous dispersion of CNTs by researchers, including physical methods with the assist of electric field,[15] magnetic field,[16-18] ultrasound[19,20] and chemical methods to treat the surface of CNTs by applying covalent bonding,[21] π–π stacking interaction,[22] surfactants,[23,24] and enzyme,[25,26] polymer matrix[27,28] and inorganic materials.[29]

Among the above mentioned methods, a win-win approach can be formed by dispersing CNTs in liquid crystals (LCs). On one hand, the overall alignment of CNTs can be controlled by the application of external fields,[30,31] on the other hand, the performance of LCs can be improved by adding very small amount of CNTs, such as enhanced thermal stability, increased dielectric anisotropy, decreased threshold voltage and accelerated electro optical response.[32,33]

According to the previous research, dispersing CNTs in nematic LC (NLC) has been systematically studied.[34] The LC-functionalized multi-walled carbon nanotubes show good miscibility with a host NLC.[35] Polyphilic promotors containing polycyclic aromatic moieties and mesogenic units are designed to stabilize the dispersion of CNTs in NLCs.[36] Organically modified laponite nanoplatelets, which show high affinity with CNTs, are used to disperse CNTs in NLC.[14]

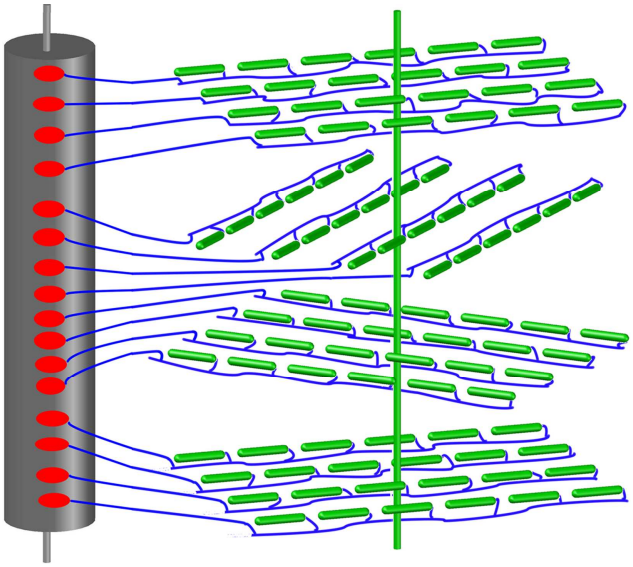

Fig. 1 Schematic illustration of the binary system consisting of CNTs and chiral surfactants ACSLCOs, the gray line and green line represent the parallel chiral axis of CNT and ACSLCO, the blue lines represent the backbone of ACSLCO, the green rods represent the chiral mesogenic units and the red ovals represent the polycyclic conjugated structure in nonmesogenic units.

In this work, for the first time, a novel method to disperse CNTs in chiral liquid crystals (CLCs) by using amphiphilic chiral side-chain liquid crystalline oligomers (ACSLCOs) as chiral surfactants is reported. The principle of structural design (as described in Fig. 1 and Fig. 2) is as follows: the backbone of side-chain liquid crystalline can improve the stability of the dispersion of CNTs with its polymer matrix physically surrounding and wrapping

This journal is © The Royal Society of Chemistry 2015

CNTs, meanwhile, the mesogenic units on oligomers chain possess affinity and miscibility with LCs for their common rod-shaped structure and similar properties; polycyclic conjugated structure in the nonmesogenic units can adhere to the surface of CNTs by π–π stacking interaction to suppress the agglomerations of neighbouring CNTs; as for the introduction of chirality into the structure of surfactant, we are aimed to build a bridge between CNTs and chiral host and to promote the compatibility between them. The novelties of this work lie in the following aspects, using chiral mesogenic unit instead of nematic mesogenic unit in the intermediary, studying the effect of mole fraction of polycyclic structure in the intermediary ACSLCO on the ability to disperse CNTs, studying the effect of dispersed CNTs on the chiral stability of CLCs.

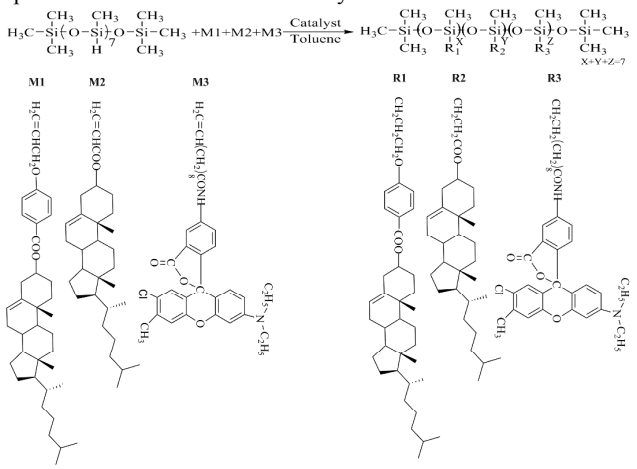

Fig. 2 Chemical structure of chiral surfactants ACSLCOs. R1 and R2 are chiral mesogenic units, R3 is nonmesogenic unit with polycyclic conjugated structure.

Table 1 Polymerization, Tc and $[\alpha]_D^{20}$ of chiral surfactants ACSLCPs.

Samples	M1 (mmol)	M2 (mmol)	M3 (mmol)	M3 (mol%)	Tc (^oC)	$[\alpha]_D^{20}$ (−)
O1	3.000	2.000	0	0	130.7	12.53
O2	2.997	1.998	0.005	0.1	129.5	12.48
O3	2.991	1.994	0.015	0.3	128.1	12.39
O4	2.985	1.990	0.025	0.5	127.3	12.28
O5	2.976	1.984	0.04	0.8	125.5	12.16
O6	2.967	1.978	0.055	1.1	124.4	12.01
O7	2.955	1.970	0.075	1.5	123.1	11.85

Experiment

Design and synthesis of chiral surfactants ACSLCOs

The design of chemical structure of novel ACSLCOs was shown in Fig. 2, the detailed synthesis process was listed in Electronic Supplementary Information. The polymerization, clearing point (Tc) and specific rotation ($[\alpha]_D^{20}$) of ACSLCOs were listed in Table 1, seven chiral surfactants (O1-O7) possessed different mole fraction of nonmesogenic units with polycyclic conjugated structure which induced π–π stacking interaction between the surface of CNT and the chiral surfactants.

Preparation of CNT-ACSLCO dispersions

The multi-walled carbon nanotubes used in this research were purchased from Shenzhen nano harbor (CVD, purity 95%, diameter 2-5 nm, length 0.5-2 μm, without functionalization). The CNT-ACSLCO dispersions were prepared by three steps, firstly, seven ACSLCO (O1-O7) solutions were prepared by adding 40 mg of ACSLCO (O1-O7) into seven vials containing 5 mL of chloroform, then, seven CNT-ACSLCO suspensions were obtained by adding 10 mg of CNTs into the above ACSLCO (O1-O7) solutions, finally, seven uniform CNT-ACSLCO dispersions were achieved by placing the above seven CNT-ACSLCO suspensions in a sonicator (25 ^oC, 100W acoustic power, 50% amplitude) for 30 minutes and centrifuging (speed 4000g) for 30 minutes to collect the upper uniform dispersions.

Preparation of CNT-ACSLCO composites

Seven homogeneous CNT-ACSLCO composites were achieved by getting rid of chloroform in seven uniform CNT-ACSLCO dispersions at 50 ^oC under vacuum.

Preparation of CLC-CNT-O7 composites

The low molecular weight CLC used in this work is S4820 (left-handed, Tc=68.3^oC), the detailed information about S4820 is listed in Electronic Supplementary Information. Firstly, a certain volume of CNT-O7 (0.85 : 8 w/w described in the section of results and discussion) dispersion was added into CLC, secondly, the composites were sonicated (25 ^oC, 100W ultrasonic power, 50% amplitude) for 30 minutes. Lastly, samples were vacuum dried at 50 ^oC to get rid of chloroform. By controlling the proportion of CLC and CNT-O7 dispersion, we obtained three composites, CLC+0.03wt%CNT+0.28wt%O7, CLC+0.06wt%CNT+0.57wt%O7 and CLC+0.1wt%CNT+0.94wt%O7, meanwhile, CLC, CLC+0wt% CNT+1wt%O7 and CLC+0.06wt%CNT+0wt%O7 were prepared as reference samples.

Characterization

The concentration of CNTs dispersed by chiral surfactants ACSLCOs was determined by fourier transform infrared (FTIR) spectrometer (PerkinElmer, Spectrum one) and ultraviolet-visible-near infrared (UV-Vis-NIR) spectrometer (PerkinElmer, lambda 950). Dispersion state of CNTs in homogeneous composites was analyzed by FTIR imaging system (PerkinElmer, Spectrum spotlight 300). Analysis of thermal phase transition was carried out in differential scanning calorimetry (DSC) equipment (TA, Q2000), temperature range: -45-160 ^oC, temperature change rate: 10 ^oC min^{-1}. Specific rotation of ACSLCOs was carried out with a PerkinElmer instrument Model341 Polarimeter (D line of a sodium vapour lamp, 589 nm, 20 ^oC, chloroform as solvent). Thermal stability was characterized by thermal gravimetric analyzer (TGA) equipment (NETZSCH, TG209C), temperature change rate was 10 ^oC min^{-1}. Observation of optical texture was conducted by using polarized optical microscope (POM) (Carl Zeiss, Scope A1) equipped with a linkam temperature controller, pictures were observed between two cross-polarizers, temperature change rate was 1 ^oC min^{-1}, the voltage signal was square wave (1000Hz). Bragg selective reflection of CLCs was measured by UV-Vis-NIR spectrophotometer (PerkinElmer, lambda 950).

This journal is © The Royal Society of Chemistry 2015

Results and discussion

FTIR spectroscopy

FTIR spectroscopy was used to try to figure out the concentration of effectively loaded CNTs in homogeneous CNT-ACSLCO dispersions. This part consisted of two sections, in the first section, a calibration curve of the FTIR absorbance versus the concentration of CNTs, which was similar with the calibration curve in UV spectroscopy was figured out, in the second section, the FTIR absorbance of effectively loaded CNTs in homogeneous CNT-ACSLCO dispersions was measured, then the concentration of effectively loaded CNTs in homogeneous CNT-ACSLCO dispersions was figured out with the assist of calibration curve in the first section.

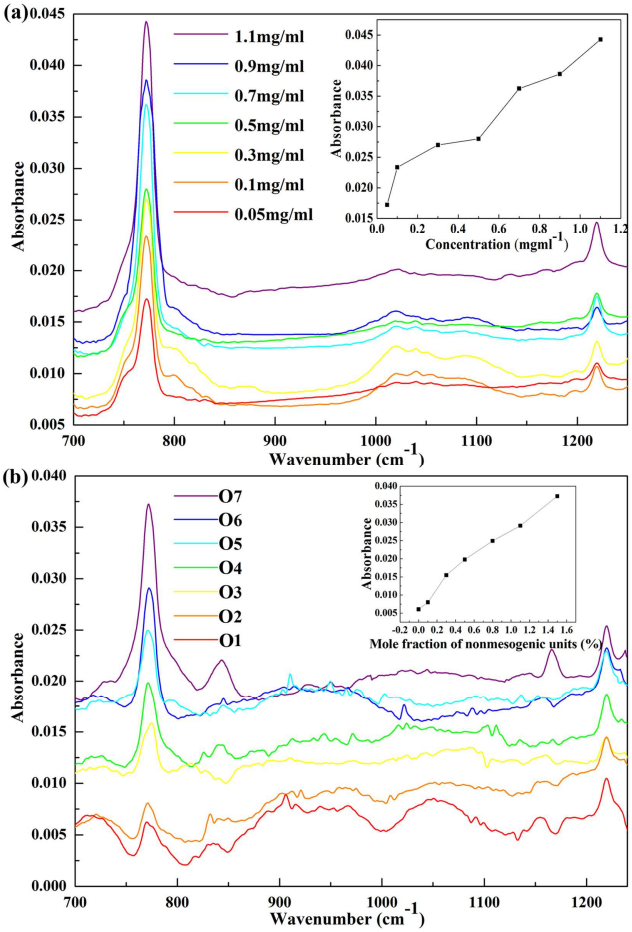

Fig. 3 (a) FTIR spectra of CNTs, inset shows the absorbance at 772 cm^{-1} versus the CNT concentration. (b) FTIR difference spectra of effectively loaded CNTs, inset shows the absorbance at 772 cm^{-1} versus mole fraction of nonmesogenic units on ACSLCOs.

In the first section, seven CNT samples were prepared by adding different amount of CNTs into 5 mL of chloroform. Then, these samples were sonicated for 30 minutes and 10 μL of the above sample was placed on a KBr film (Φ10×3 mm) to test the IR spectrum after the chloroform was completely vaporized. Result shows CNTs have strong absorption at 772 cm^{-1} whose values increase with the increase of the concentration of CNTs and weak absorption at 1219 cm^{-1} whose values have no obvious increase with the increase of the concentration of CNTs (see Fig. 3a). The inset in Fig. 3a is the calibration curve of the FTIR absorbance at 772 cm^{-1} versus the CNT concentration, but we can't establish a linear equation between the CNT concentration and absorbance due to the lack of widely recognized theory.

The second section consisted of three steps, for the first step, seven ACSLCO solutions were prepared by dissolving 40 mg of ACSLCO in 5 mL of chloroform, and 10 μL of the ACSLCO solution was placed on the KBr film to test the FTIR spectrum 1 after the chloroform was completely vaporized. For the second step, 10 μL of the homogenous CNT-ACSLCO dispersion was placed on the KBr film to test the FTIR spectrum 2. For the third step, spectrum 1 was deducted from spectrum 2 to obtain the difference spectrum, as spectrum 1 represented the FTIR absorbance of ACSLCO, spectrum 2 represented the FTIR absorbance of CNT-ACSLCO. Thus, the difference spectrum represented the FTIR absorbance of effectively loaded CNTs. The result of FTIR difference spectrum is shown in Fig. 3b, the inserted graph shows the relationship between the absorbance at 772 cm^{-1} caused by effectively loaded CNTs and different carrier ACSLCOs with the mole fraction of nonmesogenic units ranging from 0% to 1.5%. As it is hard to establish a linear equation between the CNT concentration and absorbance, we can only estimate the concentration range of CNTs in dispersion using the data in Fig. 3a. The corresponding ranges are listed in Table S1. The results suggest that the ability to disperse CNTs increases with the increase of mole fraction of nonmesogenic units, which is attributed to the increased π–π stacking interaction between the surface of CNT and the polycyclic conjugated structure in nonmesogenic units.

UV-Vis-NIR spectroscopy

UV-Vis-NIR spectroscopy was used to precisely determine the concentration of effectively loaded CNTs. This part also consisted of two sections, in the first section, a calibration curve of the absorbance versus the CNT concentration was figured out, in the second section, the absorbance of effectively loaded CNTs in homogeneous CNT-ACSLCO dispersion was measured, then the concentration of effectively loaded CNTs in homogeneous CNT-ACSLCO dispersion was precisely figured out with the assist of calibration curve in the first section.

In the first section, eight CNT solutions whose concentrations ranged from 1 μg mL^{-1} to 16 μg mL^{-1} were prepared by adding CNTs into chloroform. Their spectra (wavelength range 400-800 nm) were tested immediately after eight samples were sonicated for 30 minutes. The calibration curve was determined at 700 nm, the result is shown in Fig. 4a.

The second section consisted of three steps, for the first step, homogeneous CNT-ACSLCO dispersion was diluted 50 times to ensure the concentration was in the linear range as shown in Fig. 4a. For the second step, ACSLCO solution was prepared as reference by dissolving 40 mg of ACSLCO in 5 mL of chloroform and diluting 50 times. For the third step, the diluted CNT-ACSLCO dispersion was placed in the sample cuvette, the diluted ACSLCO solution was placed in the reference cuvette, so the absorbance was corresponding to the effectively loaded CNTs in diluted CNT-ACSLCO dispersion.

The result is shown in Fig. 4b, the absorbance gradually increase with the increase of mole fraction of nonmesogenic units on ACSLCOs, the inset shows the absorbance of loaded CNTs in diluted CNT-ACSLCO dispersions at 700 nm. According to the calibration curve in Fig. 4a, the original concentrations of CNTs in CNT-ACSLCO dispersions are calculated to be respectively 0.017 mg mL^{-1}, 0.026 mg mL^{-1}, 0.046 mg mL^{-1}, 0.092 mg mL^{-1}, 0.26 mg mL^{-1}, 0.68 mg mL^{-1} and 0.85 mg mL^{-1}. This outcome provides further confirmation to the previous observation by FTIR spectroscopy that with higher mole fraction of nonmesogenic units on ACSLCOs, the dispersion of CNTs improves.

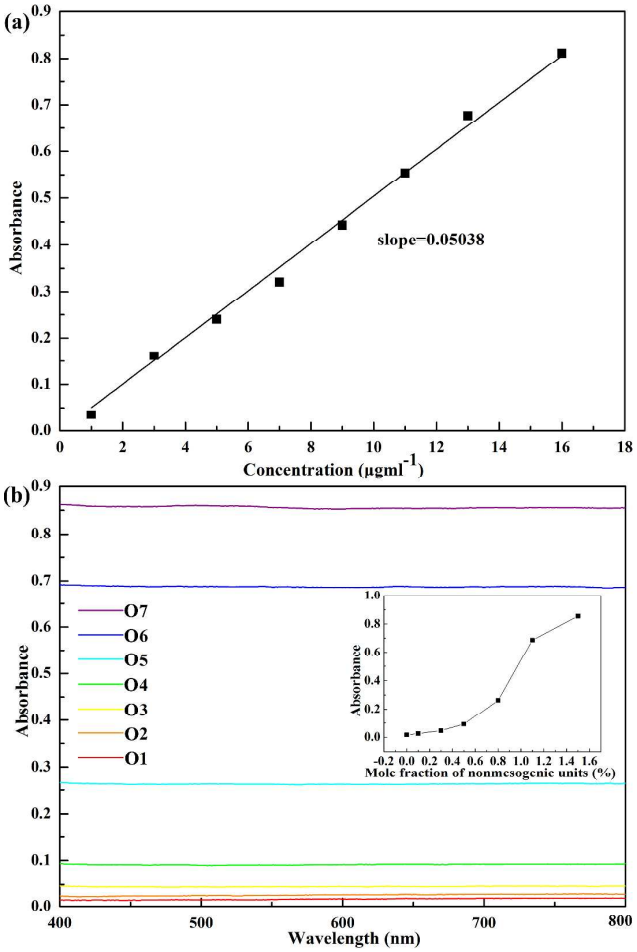

Fig. 4 (a) Calibration curves of CNTs at 700 nm. (b) UV-Vis-NIR spectra of effectively loaded CNTs in homogeneous CNT-ACSLCO dispersions after being diluted 50 times, inset shows the corresponding absorbance of effectively loaded CNTs at 700 nm versus mole fraction of nonmesogenic units on ACSLCOs.

FTIR imaging

FTIR imaging can be used to analyze the distribution of single component in multi-components by marking the characteristic IR absorption of single component in the total IR absorption of multi-components. The IR absorption of ACSLCOs and raw CNTs were firstly determined by FTIR and the result was listed in Fig. 5, CNTs have two characteristic peaks, strong absorption at 772 cm^{-1} and weak absorption at 1219 cm^{-1}, the former possesses high sensitivity which is suitable for quantification analysis, but is not suitable for qualitative analysis in this section because of the fact that ACSLCOs also have absorption at 772 cm^{-1}. Whereas the later one with lower sensitivity is not suitable for quantification analysis, but is appropriate to be used to mark CNTs in the CNT-ACSLCO composites. The total IR absorption of homogeneous CNT-ACSLCO composites were then determined by FTIR imaging system, the characteristic IR absorption of CNTs at 1219 cm^{-1} was marked in the total absorption of CNT-ACSLCO composites to figure out the dispersion state of CNTs in the composites. Results are listed in the lower part of Fig. 5, the yellow area represents stronger absorption at 1219 cm^{-1}, the green area and blue area represent weaker absorption at 1219 cm^{-1}. As 1219 cm^{-1} is the exclusive absorption peak of CNTs, it appears that CNTs are mainly dispersed in the yellow area and ACSLCOs exist in the green and blue area. We can see from Fig. 5a-d the ability of ACSLCOs to load CNTs increases with the increase of mole fraction of nonmesogenic units on ACSLCOs as the yellow area becomes larger and larger and the ability of ACSLCOs to disperse CNTs increases with the increase of mole fraction of nonmesogenic units on ACSLCOs as the yellow area becomes more and more scattered. Therefore, we can draw a conclusion that O7 is the best dispersant among O1-O7.

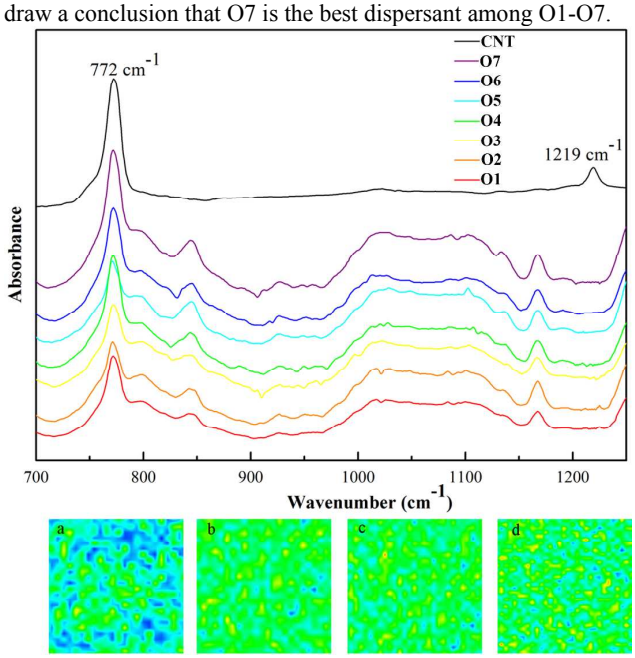

Fig. 5 The upper part is the FTIR spectra of CNTs and ACSLCOs, the lower part is the FTIR images of homogeneous CNT-ACSLCO composites, a, b, c and d are corresponding to CNT-O1, CNT-O3, CNT-O5 and CNT-O7 composites.

Thermal phase transition

The glass transition temperature (Tg) that indicates the movement of chain segment is an important parameter of side-chain liquid crystalline polymers. The Tg data of ACSLCOs are listed in Table S2 and Tg decreases with the increase of mole fraction of nonmesogenic units on ACSLCOs. The reason for this phenomenon is that Tg depends on two main factors: rigidity of the polymer main chain and intermolecular interaction between the anisotropically ordered mesogenic side chains.[37] The series of ACSLCOs have the same polymethylhydrosiloxane backbone, their difference is the mole fraction of nonmesogenic units on ACSLCOs. Furthermore, the nonmesogenic units can reduce Tg by suppressing the intermolecular interaction between the neighbouring anisotropically ordered mesogenic side chains, this is the so-called softening effect[38] which is achieved due to the increase in distance between chiral mesogenic units and the dilution of chiral mesogenic units.

In order to study the effect of CNTs on the phase transition of ACSLCOs, seven homogeneous CNT-ACSLCO composites were tested. Fig. 6 shows that Tg of CNT-ACSLCO composites (around 11 ^{o}C, the glass transition of CNT-O7 composites is not observed) are lower than that of ACSLCO (around 25 ^{o}C). The decreased Tg can be explained by the following reason: in the binary system consisting of CNT and ACSLCO (see Fig. 1), the nonmesogenic units unite with CNTs and are not confined to the LC matrix. Therefore, there is more space and larger degree of freedom for the segment on ACSLCO to move. Meanwhile, there is no additional phase-separated peak for CNT-ACSLCO composites in Fig. 6b, which indicates the dispersed CNTs do not introduce phase separation in the ACSLCO matrix.

This journal is © The Royal Society of Chemistry 2015

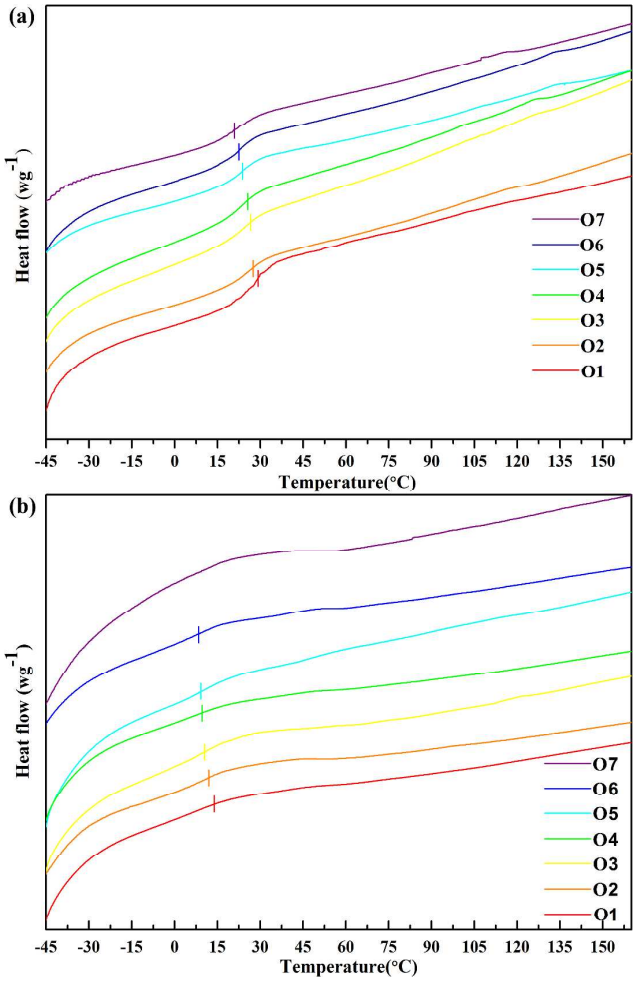

Fig. 6 (a) DSC thermograms of ACSLCOs, (b) DSC thermograms of homogeneous CNT-ACSLCO composites. The location of glass transition is presented by short rod.

Thermal stability

The thermal stability of chiral surfactants is determined by its molecular structure and the external environment. The thermal behaviors of raw CNT, O7, 2% CNT embedded O7 and 5% CNT embedded O7 were studied by TGA analysis. The preparation of 2% CNT embedded O7 composites and 5% CNT embedded O7 composites were similar with that of homogeneous CNT-ACSLCO composites. The TGA curves and first derivatives which represent the decomposition rate are plotted in Fig. 7a. Raw CNT shows excellent thermal stability within the temperature range 40 °C-400 °C, meanwhile, the onset decomposition temperatures (5% weight loss) of O7, 2% CNT embedded O7 and 5% CNT embedded O7 are 218 °C, 243.3 °C and 240.4 °C, respectively, this observation shows that CNTs enhance the thermal stability of CNT-ACSLCO composites, the increased decomposition temperatures can be attributed to both the excellent thermal stability of CNTs and their interactions with the polymer matrix .[39]

As shown in Fig. 7a, the temperature at the maximum rate of weight loss (T_{rm}) of three samples are basically the same, the reason for this outcome is that the characteristic of the thermal decomposition stems from the ACSLCO matrix. In order to obtain more detailed information concerning the decomposition process, here two key parameters are studied, Trm and the activation energy for thermal decomposition (E_a), and the following equation is established by using the Horowits-Metzger integral kinetic method for any organic pyrolysis reaction.[40]

$$\ln(-\ln w) = \frac{E_a \Delta T}{R T_{rm}^2} + k \quad (1)$$

Where w is the residual weight percentage, ΔT is defined as $\Delta T = T - T_{rm}$, R is the universal gas constant, k is the intercept of linear equation. The E_a value can be estimated from the slope of the plot of ln(-lnw) versus ΔT. The E_a of O7, 2% CNT embedded O7 and 5% CNT embedded O7 are calculated to be 96.96, 105.56 and 115.40 kJ mol^{-1} (see Fig. 7b). Higher E_a means higher energy barrier to be overcome and better thermal stability in the process of decomposition. The increased E_a can be attributed to the enhanced π–π stacking interaction between the surface of CNTs and the polycyclic conjugated system in nonmesogenic units.

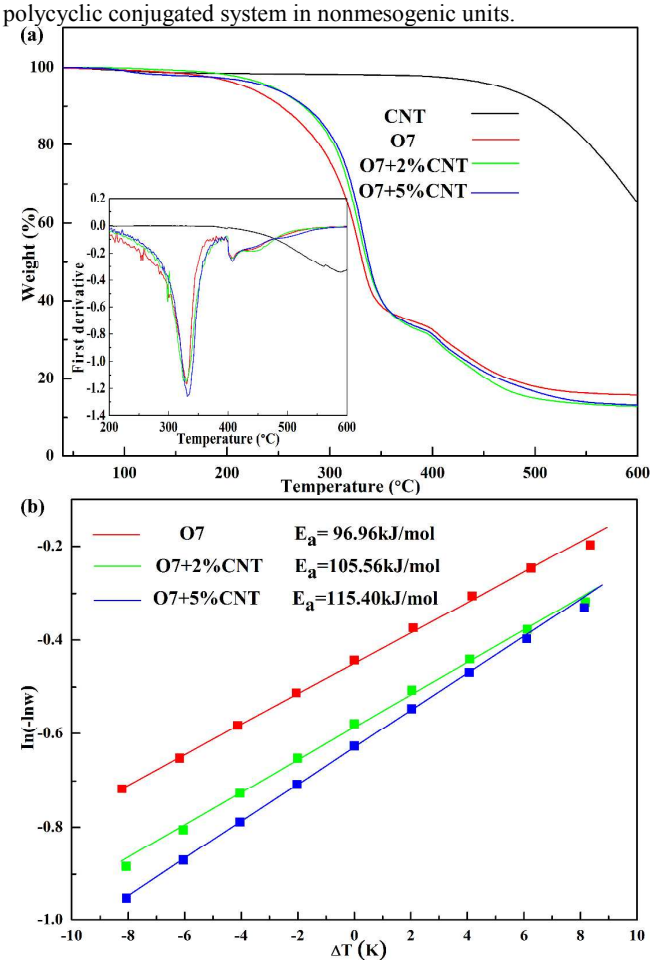

Fig. 7 (a) TGA thermographs of raw CNT, O7, 2% CNT embedded O7 and 5% CNT embedded O7, the inset shows the first derivatives of TGA curves. (b) The plots of ln(-lnw) versus ΔT for O7, 2% CNT embedded O7 and 5% CNT embedded O7.

Optical texture

POM is used to study the optical behavior of LCs by analyzing the characteristic textures of different types of LCs. All the ACSLCOs exhibit chiral grandjean texture (see Fig. 8), and the textures of ACSLCOs become more and more colorless and gray with the increase of mole fraction of nonmesogenic units on ACSLCOs. The fading of liquid crystalline behavior can be attributed to the fact that the nonmesogenic units disturb the molecular arrangement of chiral mesogenic units.

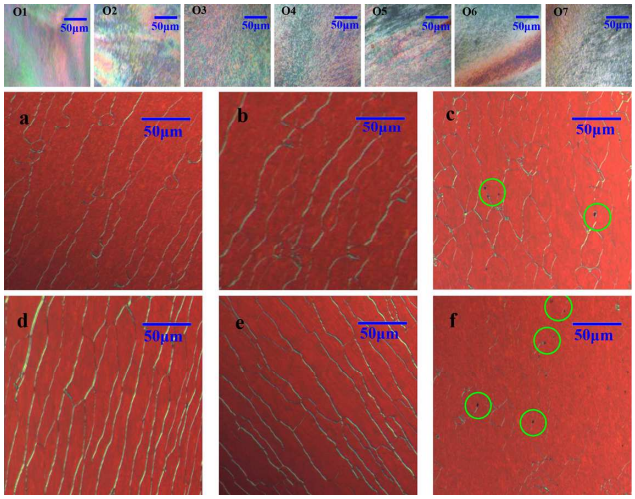

Fig. 8 The upper part belongs to the optical textures of ACSLCOs at 100 °C, the lower part (a-f) belongs to CLC, CLC+0wt%CNT+1wt %O7, CLC+0.06wt%CNT+0wt%O7, CLC+0.03wt%CNT+0.28wt %O7, CLC+0.06wt%CNT+0.57wt%O7 and CLC+0.1wt%CNT+ 0.94wt%O7 at 25 °C, the CNT aggregations are delineated by green circles (crossed polarizers, 200×).

In order to study the effect of chiral surfactants on building a bridge between CNTs and chiral materials and promoting the compatibility between them, a ternary system was constructed by CNT, chiral surfactant O7 and low molecular weight CLC. POM can be acted as an effective method to characterize the dispersion state of nanoparticles in composites.[30,31] As shown in Fig. 8a and b, CLC exhibits the same planar oily streak texture as CLC+0wt%CNT+1wt %O7. This phenomenon indicates that O7 possesses good compatibility with CLC, the reason for this outcome is that the mesogenic units on chiral surfactant O7 tend to join the CLC matrix. However, there are CNT aggregations in the texture of CLC+0.06wt %CNT+0wt%O7 due to the interaction between neighbouring CNTs. There are no CNT aggregations in Fig. 8d and e, which indicates that CNTs have excellent compatibility with CLCs with the assist of O7, this effect is caused by the amphiphilic O7, on one hand, the mesogenic units on O7 make O7 have good affinity with CLCs, on the other hand, the polycyclic conjugated structure in nonmesogenic units makes O7 possess affinity with CNTs (see Fig. 10 field off state).

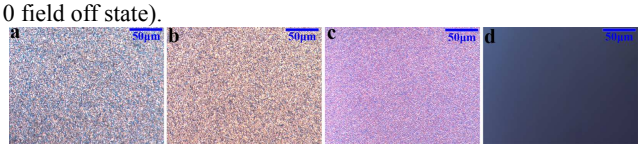

Fig. 9 The optical textures of CLC+0.06wt%CNT+0.57wt%O7 under electric field, a-c (focal conic state) are corresponding to 5v, 15v, 25v, d (field-induced homeotropic state) is corresponding to 40v.

However, there is side effect when the concentration of CNTs in CLC-CNT-O7 composites reaches 0.1% (see Fig. 8f) due to the fact that the dispersion of CNTs in CLC is saturated. Meanwhile, the optical textures in Fig. 9 show there are no CNT aggregations in the composite of CLC+0.06wt%CNT+0.57wt%O7 under electric field, indicating that chiral surfactant O7 can also promote the dispersion of CNTs in LC matrix under electric field (see Fig. 10 field on state).

O1 without R3 and O8 without R1 and R2 were also used to disperse CNTs in CLC matrix. Both O1 and O8 fail to disperse CNTs in CLC matrix, there are CNT aggregations and no O1 aggregations in Fig. 11a, this result is attributed to the following reason, on one hand, the chiral liquid crystalline side chains on O1 have affinity with CLC and help O1 dissolve in CLC, on the other hand, CNTs tend to bundle and cluster together in disordered agglomerates because of lack of pi-stacking unit R3. Fig. 11b shows that there are CNT aggregations and O8 aggregations in CLC, the reason for this outcome is that O8 possesses poor solubility in CLC when having no chiral liquid crystalline side chains, and the pi-stacking units in O8 aggregations fail to be effectively used to disperse CNTs. The above-mentioned results indicate that both chiral liquid crystalline side chains and pi-stacking side chains are necessary to disperse CNTs in CLC matrix.

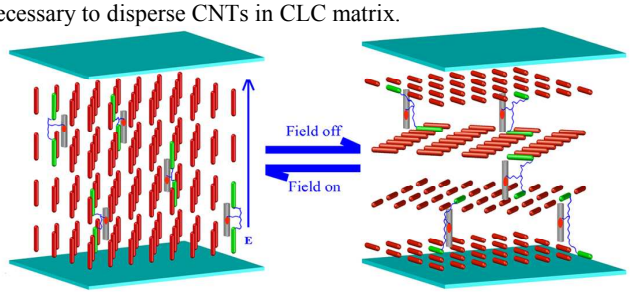

Fig. 10 Schematic illustration of electrically controlled orientational switch of ternary system consisting of CNT, O7 and low molecular weight CLC. The red rods represent CLCs, the green rods represent chiral mesogenic units on ACSLCOs, the red ovals represent the polycyclic conjugated structure in nonmesogenic units and the blue lines represent the backbone of ACSLCOs. ACSLCOs promote the dispersion of CNT into CLC matrix in both field-on and field-off states with their polycyclic conjugated structure anchoring on the surface of CNT and chiral mesogenic units joining the CLC matrix.

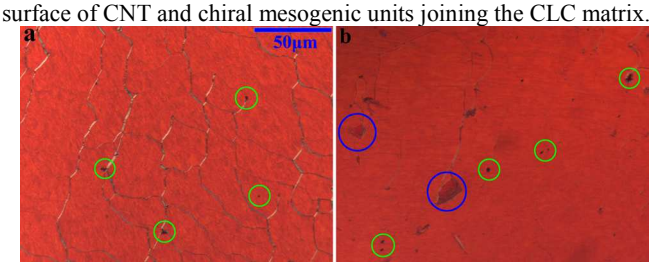

Fig. 11 Optical textures of CLC+0.03wt%CNT+0.28wt%O1 (a), CLC+0.03wt%CNT+0.28wt%O8 (b) at 25 °C. The dark CNT aggregations are delineated by green circles, the dark red O8 aggregations are delineated by blue circles (crossed polarizers, 200×).

Bragg selective reflection

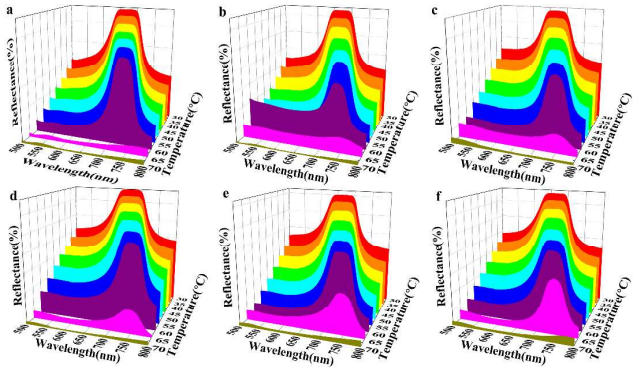

Fig. 12 Bragg selective reflection spectra (a-f) of CLC, CLC+0wt% CNT+1wt%O7, CLC+0.01wt%CNT+0.094wt%O7, CLC+0.03wt% CNT+0.28wt%O7, CLC+0.06wt%CNT+0.57wt%O7 and CLC+0.08 wt%CNT+0.75wt%O7. Temperature ranges from 30 °C to 70 °C.

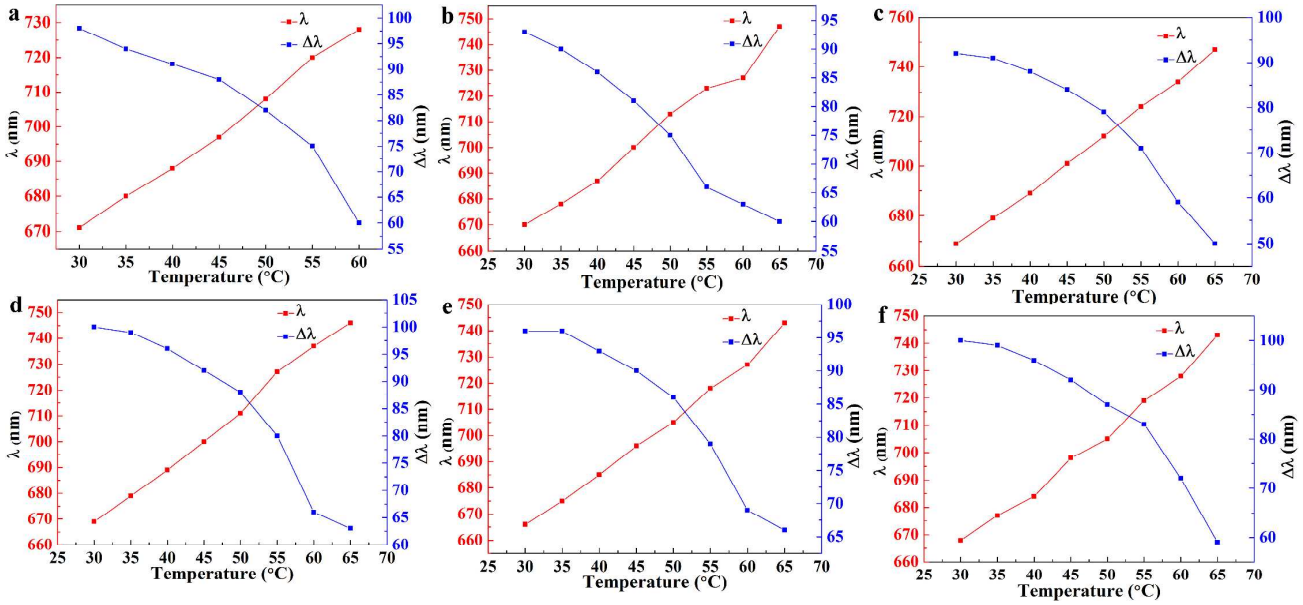

Fig. 13 λ and Δλ of bragg selective reflection spectra (a-f) of CLC, CLC+0wt%CNT+1wt%O7, CLC+0.01wt%CNT+0.094wt%O7, CLC+0.03wt%CNT+0.28wt% O7, CLC+0.06wt%CNT+0.57wt%O7 and CLC+0.08wt%CNT+0.75wt%O7.

CLCs can be considered as a one-dimensional photonic crystal,[41] bragg selective reflection is one of the unique properties of CLCs with a periodic helical molecular structure.[42-44] The reflection light wavelength (λ) from the helical structure is described by Bragg's law listed in equation 2,[45] where $\bar{n}$ is the average refractive index and P is the pitch length of CLCs (the distance of the helical structure undergoing a 360° twist), meanwhile, the reflection bandwidth (Δλ) is given by equation 3,[46] where Δλ is the birefringence.

$$\lambda = \bar{n}P \quad (2)$$

$$\Delta\lambda = \Delta nP \quad (3)$$

As bragg selective reflection is determined by the chirality of CLC, better stability of chirality means better stability of bragg selective reflection. In this section, we studied the effect of dispersed CNTs on the chiral stability of chiral host CLC by characterizing the effect of dispersed CNTs on the bragg selective reflection of chiral host CLC. Four CLC-CNT-O7 composites were prepared, CLC+0.01wt%CNT+0.094wt%O7, CLC+0.03wt% CNT+0.28wt% O7, CLC+0.06wt%CNT+0.57wt%O7 and CLC+0.08wt%CNT+0.75 wt%O7 respectively, CLC and CLC+0wt%CNT+1wt%O7 were studied as reference samples. We can draw four conclusions from Fig. 12 and Fig. 13. Firstly, λ makes a red shift with the increase of temperature for all the samples, the reason for this outcome is that helical structure starts to unwind and chirality weakens. Secondly, Δλ becomes narrowed as temperature increases, this is because the transition from anisotropy to isotropy leads to smaller Δn and more narrowed Δλ according to equation 3. Thirdly, the selective reflection of CLC disappears when temperature reaches 65 °C, however, there is still weak reflection for CLC+0wt%CNT+1wt%O7, the reason for this phenomenon is that the higher Tc of O7 broadens the temperature range of cholesteric phase of CLC. Lastly but most important, the reflections in Fig. 12c-f are more obvious than that in Fig. 12b at 65 °C even if the corresponding O7 concentration of Fig. 12b is far more than the corresponding O7 concentrations of Fig. 12c-f, this indicates that the enhanced reflection stability in Fig. 12c-f is not caused by O7, this means the increased chiral stability of CLC is attributed to the dispersed CNTs, which brings extra stability to the helical structure of CLC at higher temperature.

Conclusions

In order to broaden the extensive and unforeseeable application of CNTs in the field of composite materials, we have proposed a novel and effective dispersion method through designing chiral surfactants ACSLCOs, the dispersion model is expressed as a binary system consisting of CNTs and ACSLCOs. The quantity of loaded CNTs by ACSLCOs increases when increasing the mole fraction of polycyclic conjugated structure on ACSLCOs. Higher mole fraction of polycyclic conjugated structure induces better dispersion effect. The homogeneously dispersed CNTs can reduce the phase transition temperature and improve the thermal stability of ACSLCOs as a result of the interaction between CNTs and ACSLCOs. To further study the properties and applications of the homogeneous CNT-ACSLCO composites in chiral host, a ternary chiral system is constructed by CNT, O7 and low molecular weight CLC. CNTs possess excellent miscibility with low molecular weight CLCs with the assist of chiral surfactants O7 when the CNT concentration is less than 0.1%. Meanwhile, the dispersed CNTs can strengthen the chiral stability of CLCs. We believe that the design and synthesis of chiral surfactants to build a bridge between CNTs and chiral materials will be a promising topic for researchers to broaden the potential applications of CNTs in the field of chiral materials, such as chemical asymmetric synthesis, biomaterials, blue phases and liquid crystal displays. At the same time, it is worthwhile mentioning that the dispersion concentration of CNTs in low molecular weight CLCs is less than 0.1%, which can limit the applications of CNTs. In view of this, our further studies will be focused on the search of other types of functional materials to promote better dispersion of CNTs.

Acknowledgments

The authors are grateful to National Natural Scientific Fundamental Committee of China and the Minister of Science and Technology of China for financial support of this work.

Notes and references

Center for Molecular Science and Engineering, Northeastern University, 3 Wenhua Road, Shenyang 110819, P. R. China
*Corresponding author: Baoyan Zhang (E-mail: neuchem@126.com)

[1] S. Iijima, *Nature*, 1991, **354**, 56-58.
[2] G. L. Che, B. B. Lakshmi, E. R. Fisher, C. R. Martin, *Nature*, 1998, **393**, 346-349.
[3] E. Frackowiak, F. Beguin, *Carbon*, 2002, **40**, 1775-1787.
[4] W. Q. Fu, L. Liu, K. L. Jiang, Q. Q. Li, S. S. Fan, *Carbon*, 2010, **48**, 1876-1879.
[5] J. M. Schnorr, T. M. Swager, *Chem Mater*, 2010, **23**, 646-657.
[6] S. J. Kang, C. Kocaba, T. Ozel, M. Shimi, N. Pimparkar, M. A. Alam, S. V. Rotkin, *Nature nanotechnology*, 2007, **2**, 230-236.
[7] C. Wang, J. C. Chien, K. Takei, T. Takahashi, J. Nah, A. M. Niknejad, A. Javey, *Nano Lett*, 2012, **12**, 1527-1533.
[8] Z. Liu, S. M. Tabakman, Z. Chen, H. J. Dai, *Nature Protocols*, 2009, **4**, 1372-1381.
[9] B. C. Satishkumar, L. O. Brown, Y. Gao, C. C. Wang, H. L. Wang, *Nature nanotechnology*, 2007, **2**, 560-564.
[10] S. Hitosugi, A. Matsumoto, Y. Kaimori, R. Iizuka, K. Soai, H. Isobe，*Org. Lett.*, 2014, **16**, 645-647.
[11] T. Premkumar, R. Mezzenga, K. E. Geckeler, *Small*, 2012, **8**, 1299-1313.
[12] Y. Ji, J. E. Marshall, E. M. Terentjev, *Polymers*, 2012, **4**, 316-340.
[13] P. C. Luo, H. Wu, M. Morbidelli, *Carbon*, 2014, **68**, 610-618.
[14] O. Yaroshchuk, S. Tomylko, O. Kovalchuk, N. Lebovka, *Carbon* 2014, **68**, 389-398.
[15] S. J. Jeong, K. A. Park, S. H. Jeong, H. J. Jeong, C. Nah, K. H. An, D. Pribat, S. H. Lee, Y. Hee, *Nano Lett*, 2007, **7**, 2178-2182.
[16] M. D. Lynch, D. L. Patrick, *Nano Lett*, 2002, **2**, 1197-1201
[17] B. W. Smith, Z. Benes, D. E. Luzzi, *Appl. Phys. Lett.*, 2000, **77**, 663-665.
[18] J. Hone, M. C. Llaguno, N. M. Nemes, *Appl. Phys. Lett.*, 2000, **77**, 666-668.
[19] Y. Z. You, J. J. Yan, Z. Q. Yu, M. M. Cui, C. Y. Hong, B. J. Qu, J. *Mater. Chem.*, 2009, **19**, 7656-7660.
[20] M. Nadler, T. Mahrholz, U. Riedel, C. Schilde, A. Kwade, *Carbon*, 2008, **46**, 1384-1392.
[21] R. Vukicevic, I. Vukovic, H. Stoyanov, A. Korwitz, D. Pospiech, G. Kofod, K. Loos, G. T. Brinke, S. Beuermann, *Polym. Chem.*, 2012, **3**, 2261-2265.
[22] R. R. Johnson, A. T. C. Johnson, M. L. Klein, *Nano Lett*, 2008, **8**, 69-75.
[23] Y. Lin, S. Taylor, H. P. Li, K. A. S. Fernando, L. W. Qu, W. Wang, L. R. Gu, B. Zhou, Y. P. Sun, *J. Mater. Chem.*, 2004, **14**, 527-541.
[24] J. R.Yu, N. Grossiord, C. E. Koning, J. Loos. *Carbon*, 2007, **45**, 618-623.
[25] B. G. Cousins, A. K. Das, R. Sharma, Y. N. Li, J. P. McNamara, I. H. Hillier, I. A. Kinloch, R. V. Ulijn, *Small*, 2009, **5**, 587-590.
[26] K. Besteman, J. O. Lee, F. G. M. Wiertz, H. A. Heering, C. Dekker, *Nano Lett*, 2003, **3**, 727-730.
[27] P. Imin, F. Y. Cheng, A. Adronov, *Polym. Chem.*, 2011, **2**, 411-416.
[28] E. Pavoni, E. Bandini, M. Benaglia, J. K. Molloy, G. Bergamini, P. Ceroni, N. Armaroli, *Polym. Chem.*, 2014, **5**, 6148-6150.
[29] H. B. Chu, L. Wei, R. L. Cui, J. Y. Wang, Y. Li, *Coordin. Chem. Rev.,* 2010, **254**, 1117-1134.
[30] I. Dierking, G. Scalia, P. Morales, *J. Appl. Phys.*, 2005, **97**, 044309-5.
[31] I. Dierking, G. Scalia, P. Morales, D. Leclere, *Adv. Mater.*, 2004, **16**, 865-869.
[32] R. Basu, G. S. Iannacchione, *Appl. Phys. Lett.*, 2009, **95**, 173113.
[33] H. Y. Chen, W. Lee, N. A. Clark, *Appl. Phys. Lett.*, 2007, **90**, 033510.
[34] Schymura S, Kühnast M, Lutz V, Jagiella S, Weglikowska UD, Roth S, F. Giesselmann, C. Tschierske, G. Scalia, J. Lagerwall, *Adv Funct Mater*, 2010, **20**, 3350-3357.
[35] H. J. Yoo, S. Y. Lee, N. H. You, D. S. Lee, H. Yeo, Y. M. Choi, M. Goh, J. Park, K. Akagi, J. W. Cho, *Synthetic. Met.*, 2013, **181**, 10-17.
[36] M. Kühnast, C. Tschierske, J. Lagerwall, *Chem. Commun.*, 2010, **46**, 6989-6991.
[37] H. Finkelmann, G. Rehage. Liquid Crystal Side Chain Polymers, Springer, Berlin, 1984, pp. 152.
[38] H. Finkelmann, G. Rehage. Liquid Crystal Side Chain Polymers, Springer, Berlin, 1984, pp. 153.
[39] J. W. Xiong, Z. Zheng, X. M. Qin, M. Li, H. Q. Li, X. L. Wang, *Carbon*, 2006, **44**, 2701-2707.
[40] J. Y. Kim. *Materials*, 2009, **2**, 1955-1974.
[41] M. Mitov, E. Nouvet, N. Dessaud, *Eur. Phys. J. E: Soft Matter and Biological Physics*, 2004, **15**, 413-419.
[42] H. L. De Vries, *Acta Crystallogr*, 1951, **4**, 219-26.
[43] D. W. Berreman, T. J. Scheffer, *Phys. Rev. Lett.*, 1970, **25**, 577.
[44] F. D. Saeva, J. J. Wysocki, *J. Am. Chem. Soc.*, 1971, **93**, 5928-5929.
[45] J. Ma, Y. N. Li, T. White, A. Urbas, Q. Li, *Chem. Commun.*, 2010, **46**, 3463-3465.
[46] M. Mathews, R. S. Zola, S. Hurley, D. K. Yang, T. J. White, T. J. Bunning, *J. Am. Chem. Soc.*, 2010, **132**, 18361-18366.

 This journal is © The Royal Society of Chemistry 2015